Logarithmic Sensing in *Escherichia coli* Bacterial Chemotaxis

Yevgeniy V. Kalinin,[†] Lili Jiang,[‡] Yuhai Tu,[§*] and Mingming Wu[†¶*]
[†]School of Chemical and Biomolecular Engineering, Cornell University, Ithaca, New York 14853; [‡]Center for Theoretical Biology and School of Physics, Peking University, Beijing 100871, China; [§]IBM T. J. Watson Research Center, Yorktown Heights, New York 10598; and [¶]Sibley School of Mechanical and Aerospace Engineering, Cornell University, Ithaca, New York 14853

ABSTRACT We studied the response of swimming *Escherichia coli* (*E. coli*) bacteria in a comprehensive set of well-controlled chemical concentration gradients using a newly developed microfluidic device and cell tracking imaging technique. In parallel, we carried out a multi-scale theoretical modeling of bacterial chemotaxis taking into account the relevant internal signaling pathway dynamics, and predicted bacterial chemotactic responses at the cellular level. By measuring the *E. coli* cell density profiles across the microfluidic channel at various spatial gradients of ligand concentration *grad*[*L*] and the average ligand concentration $\overline{[L]}$near the peak chemotactic response region, we demonstrated unambiguously in both experiments and model simulation that the mean chemotactic drift velocity of *E. coli* cells increased monotonically with *grad* [*L*]/$\overline{[L]}$ or ~*grad*(log[*L*])—that is *E. coli* cells sense the spatial gradient of the logarithmic ligand concentration. The exact range of the log-sensing regime was determined. The agreements between the experiments and the multi-scale model simulation verify the validity of the theoretical model, and revealed that the key microscopic mechanism for logarithmic sensing in bacterial chemotaxis is the adaptation kinetics, in contrast to explanations based directly on ligand occupancy.

INTRODUCTION

Sensory systems in higher organisms (e. g., human vision and hearing) can sense the relative change of the stimuli, which is known as the Weber law (1). In 1972, Dahlquist and co-workers suggested that bacteria might also respond to the relative change of the chemical concentration (2). Using mixing chambers, they created different spatial ligand profiles (both linear and exponential) and studied the density distribution of the swimming bacteria. The density distribution was measured by the intensity of scattered laser light. Later work by Mesibov and co-workers introduced the classical capillary assays to study bacterial chemotaxis (3). In the work of Mesibov et al., capillary tubes with different ligand concentrations were introduced to the bacterial suspension and the chemotactic response was characterized by the number of bacteria collected in the capillary tube at a given time. Experimental results from the capillary assay and the mixing chamber both suggested that bacteria responded to the relative change of the ligand concentration. However, neither the mixing chambers nor the capillary assays provided a well-controlled and easily quantifiable concentration profile. In particular, the ligand profiles in these early experiments could change significantly within the time needed for observing chemotaxis behavior, thus making quantitative analysis of the phenomenon very difficult. As a result, the nature, as well as the range, of the logarithmic sensing was not well determined experimentally. In 1974, Brown and Berg (4) studied the responses of bacteria to the temporal change of the ligand concentration using a tracking microscope, where the track of an individual bacterium was recorded. The chemotactic responses were characterized by the average run time of the tracked bacteria. The experimental results of Brown and Berg were fit to a theoretical model based on the receptor binding kinetics. They suggested that the bacterial chemotactic sensitivity is proportional to the change in ligand binding,

$$\Delta\left(\frac{[L]}{[L]+k_d}\right)\approx\frac{k_d[L]}{([L]+k_d)^2}\times\frac{\Delta[L]}{[L]},$$

which is determined by the ligand concentration $[L]$ and the fixed dissociation constant k_d. Since $\frac{k_d[L]}{([L]+k_d)^2}$ is roughly constant when $[L]\approx k_d$, the chemotactic sensitivity is proportional to $\Delta[L]/[L]$. The bacteria sense the relative changes of the ligand concentration. It is easy to see that this argument only works in a very narrow region of ligand concentration around k_d, whereas it is now well accepted that the chemotactic sensitivity extends over several decades of ligand concentrations (3,5). Molecularly, this argument was made totally independent of adaptation in the signaling pathway, which we now know is crucial to the cell's ability to sense and then to follow a gradient in a wide range of concentration background.

Since the early explorations of this very important problem of bacterial logarithmic sensing, major developments have occurred recently in both our ability to establish well-controlled spatial and temporal ligand profiles at the micrometer length scale for the studies of bacterial chemotaxis at cellular level (6,7) and our understanding of the bacterial chemotaxis signaling pathway at the molecular level (8–11). On the technology side, microfluidic devices have shown great promise for cell-based assays due to their size proximity to cells, compatibility with optical

Submitted July 17, 2008, and accepted for publication October 28, 2008.

*Correspondence: mw272@cornell.edu; yuhai@us.ibm.com

Editor: Jason M. Haugh.

0006-3495/09/03/2439/10 $2.00

doi: 10.1016/j.bpj.2008.10.027

microscopes, and the ease with which one can precisely control the cells' chemical and mechanical environment (7,12,13). In addition, the current state of art imaging technology has allowed us to follow the motion of multiple swimming bacteria in real time and in three-dimensional space (14,15). Recently, we have developed a hydrogel-based microfluidic chemotaxis device that is able to generate a steady and linear chemical gradient in a microfluidic channel. Initial experiments have been conducted successfully in the quantitative studies of directed cell migration both for suspension (bacteria) and adherent (neutrophils and neural stem cells) cells (16,17). On the biology side, the molecular architecture (the molecular players and their interactions) of the chemotaxis pathway has been worked out (10,11,18,19) and various mathematical models have been developed to describe different aspects of this signaling pathway (8,9) over the last decade. Most recently, in vivo measurements of the kinase activity in response to different levels of external signals in different backgrounds have been made using fluorescence resonance energy transfer (FRET) (20–22). These quantitative measurements have led to, and can be explained by, a comprehensive mathematical model that takes into account the relevant biology, in particular the receptor-receptor interaction (23–28) and the appropriate methylation kinetics that is required for (near) perfect adaptation (29–31). This quantitative model with its parameters determined from the microscopic experiments, such as the in vivo measurements of kinase activity by FRET, can then be used to predict quantitatively the behavior of cells in response to different stimuli and to understand the molecular mechanism for various interesting cellular behaviors.

In this work, we use a systems-biology approach in which we integrate quantitative experiments with the multi-scale theoretical modeling that takes into account the relevant internal signaling transduction pathway. The newly developed engineering tools (microfluidics and a particle tracking imaging technique), in combination with the high efficiency coarse-grained theoretical modeling, allow us for the first time, to our knowledge, to demonstrate explicitly that the average chemotactic drift velocity depends on the spatial gradient of the logarithm of the ligand concentration, and to determine the range of logarithmic sensing for both MeAsp(α-methyl-DL-aspartate) and L-Serine. The prediction of our model based on simulation of the (microscopic) molecular pathway with all parameters obtained from independent in vivo response data (i.e., with no free parameters) agrees quantitatively with the experimental results for all ranges of ligand (MeAsp) profiles. This agreement verifies the validity of the multi-scale theoretical model. More importantly, this combined approach of experiments and theoretical modeling enables us to understand the molecular mechanism of the observed cellular level phenomena. In particular, we find that the logarithmic sensing in bacterial chemotaxis is caused by the adaptation kinetics. By fitting the theoretical model to experimental data, we also determined microscopic parameters for Tsr receptor in response to L-Serine that are currently not available in the literature.

METHODS

Cell preparation

Escherichia coli (*E. coli*) cells (RP437 strain, a gift from Sandy Parkinson, the University of Utah, transformed with pTrc-GFP plasmid in DeLisa lab, Cornell University) were grown in Tryptone Broth (10.0 g/L of Bacto Tryptone powder dissolved in phosphate-buffered saline (PBS)) supplemented with 100 μg/ml Ampicillin in a shaker bath at 30°C, 150 rpm. The overnight cultures were inoculated the next morning in a fresh Tryptone Broth medium (~25X) to a final concentration that corresponds to OD_{600}~0.05. Inducer isopropyl thiogalactopyranoside was added to a final concentration of 1 mM when cell density reached OD_{600}~0.2. Cells were harvested at exponential growth phase when OD_{600} reached ~0.5. Cells were resuspended twice (centrifuged at 1500 g for 2 min) in chemotaxis buffer (PBS/0.1 mM EDTA/1μM methionine/10 mM lactic acid, pH =7.3) before experiments. For all the experiments shown here, the final cell density was ~1.5×10^8 cells/mL. Within the same day, we used the same overnight culture for up to three subcultures in a time gap of ~2 h (it took ~2 h for one experimental run) to ensure that each experimental run used cells with exact same preparation procedures as described above.

Microfluidic device design and calibrations

A microfluidic device was constructed to provide a linear and stable chemical gradient in a microfluidic channel where cells were seeded. Details of the device can be found in references (17,32). Briefly, we first made positive relief features (four three-channel devices) on a silicon master using the standard photolithography technique at the Cornell NanoScale Science and Technology Facility. Hydrogel replicas of the device can then be made repeatedly using the same master. It involved pouring 3% hot agarose gel (0.3g agarose, 10ml PBS) onto the silicon master surrounded by a 1 inch × 3 inch polydimethylsiloxane (PDMS) ring spacer of 1mm thickness, and then peeling it off once it was gelled in room temperature. The gelled membrane was soaked in a chemotaxis buffer for at least 30 min before being used and can be stored for up to a week. Before each experiment, the patterned membrane was sandwiched between a plastic manifold and a glass slide (1 inch × 3 inch) supported by a stainless steel frame. The plastic manifold was predrilled with all the inlets and outlets for the microfluidic channels. The flows in the sink and source channels were provided by either a syringe pump (Harvard Apparatus PHD2000; Harvard Apparatus, Holliston, MA) or a peristaltic pump (Watson Marlow 205S with eight parallel lines; Watson Marlow, Wilmington, MA). There are four three-channel devices (such as the one shown in Fig. 1 *a* in one chip. This is important for conducting four parallel experiments using cells from the same batch.

Experimental strategies are described in Fig. 1 *a*. Three parallel channels (dimension 400μm wide, 160 μm depth and 12 mm long) were patterned on an agarose membrane of 1 mm thickness. The channels were separated by an agarose gel ridge of 250 μm width. When the chemical attractant of high and low concentrations flowed through the source and the sink channel respectively, the chemical diffused through the agarose gel (with a diffusion coefficient similar to that of water) from the source channel to the sink channel. A linear chemical gradient was established in the center channel once a steady state was reached. The cells were seeded in the center channel and responses of the cells to the chemical gradients were recorded (Fig. 1, *b–d*).

To calibrate the device, we used a 100 μM fluorescein (360Da molecular weight mass, Sigma, St. Louis, MO) solution. Fig. 1 *a* is a fluorescent image of the three channel device with fluorescein solution in the source channel and blank buffer in the sink channel. A linear light intensity profile was established from the source channel to sink channel with poor visibility of the agarose ridge indicating that the diffusion coefficients of fluorescein through

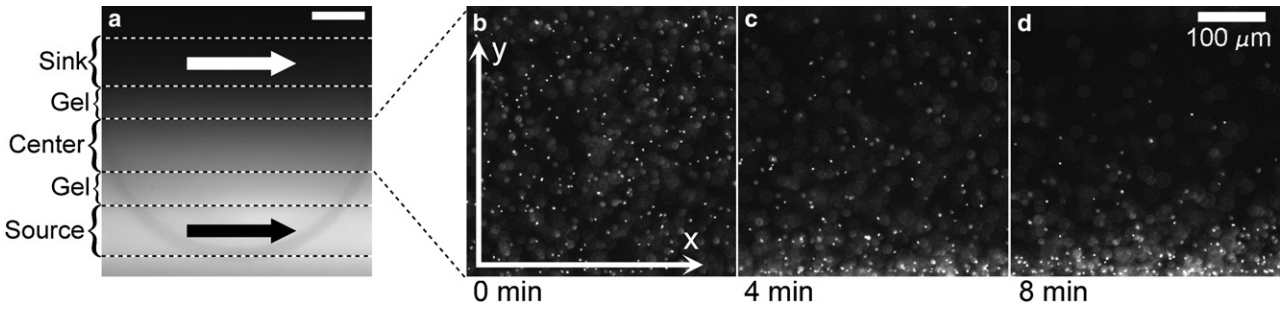

FIGURE 1 Chemotactic responses of *E. coli* in a linear chemical gradient. (*a*). A fluorescent micrograph of the middle portion of the microfluidic device. Shown in the image are three channels patterned in agarose gel, each is 400 μm wide and 160 μm deep. A 100 μM fluorescein solution is flowing in the source channel, while a blank buffer is flowing in the sink channel. The scale bar shown is 400 μm. (*b–d*). A time sequence of images of swimming *E. coli* located in the center channel of the microfluidic device. t = 0 is the time when chemo-attractant MeAsp of 100 μM and a blank buffer starts flowing in the source and sink channel, respectively.

water and agarose gel are very close (for details, see Fig. 2 *c* and (17)). This linear gradient can be maintained indefinitely as long as the flows in the sink/source channels were kept a constant (5 μL/min in our case). It should be noted that devices have also been calibrated with *E. coli* present in the center channel and it was found that the presence of bacteria did not affect the diffusion coefficient of the fluorescent dye. This was demonstrated by the linear nature of the fluorescent intensity profile from the source to the sink channel with the slope across the center channel in the presence of the bacteria equal to the slope across the agarose ridge (data not shown).

Data acquisition and imaging

For each experimental run, we performed four parallel experiments at four different chemical concentrations using four devices on the same chip. First, we seeded cells in four center channels by injecting cell culture with a gel-loading pipette tip, and sealed all the inlet and outlet to avoid through flow in the center channel. To prevent slow flow in the center channel, it is critical that the PDMS spacer has a uniform thickness and all of the tubing used is exactly identical to avoid unwanted pressure differences between the inlet and outlet, or sink and source channel. L-Serine and MeAsp of high and low concentrations were then pumped through the source and sink channels respectively at a rate of 5 μL/min. Four movies were taken consecutively of the four center channels at ~20 min after the start of the flow in the sink and source channels. A typical movie has 500 frames recorded at 10 frames per second and each image is 410 μm × 410 μm in size. A fluorescent microscope (Olympus IX 51, 20X objective lens, (Olympus, Center Valley, PA) EXFO X-Cite 120 Fluorescence Illumination System (EXFO, Ontario, Canada)) and a CCD camera (Cascade 512B camera; Photometrics, Tucson, AZ) were used for imaging.

Data analysis

To quantify the bacterial chemotactic response, we first tracked the (x_i,y_i) positions of the swimming bacteria in the mid 95% portion of the center channel (an area of 380 μm × 410 μm) using an in house particle tracking software (available at our lab website http://biofluidics.mae.cornell.edu) (Fig. 2 *b*). Here, *i* is the index of the bacterium being tracked, and (0,0) is defined as the left lower corner of the center channel as shown in Fig. 1 *b*. These positions were subsequently used to form tracks using the standard nearest neighbor method. Using tracked positions, we then calculated (1) the chemotactic migration coefficient (CMC) of the swimming bacteria in the channel (7, 32). CMC is the average *y* position of all the cells being tracked with respect to the center position of the channel. Here, CMC=(mean $(y_i) - y_c$)/190 μm, where $y_c$is the *y* coordinate at the center of the channel, 190 μm is the half width of the channel being tracked; (2) normalized cell density distribution $p(y)$ across the channel. For each movie series, we calculated CMCor $p(y)$ for each of the 500 images first, and then obtained an average value. For those data taken in the high chemotactic response region, the probability density function was fitted to an exponential decay function with two adjustable parameters. Using bacterial tracks, we computed motility constant μ by fitting the velocity auto-correlation function to an exponential decay function. For more details of this computation, please refer to the work of Liao et al. (33).

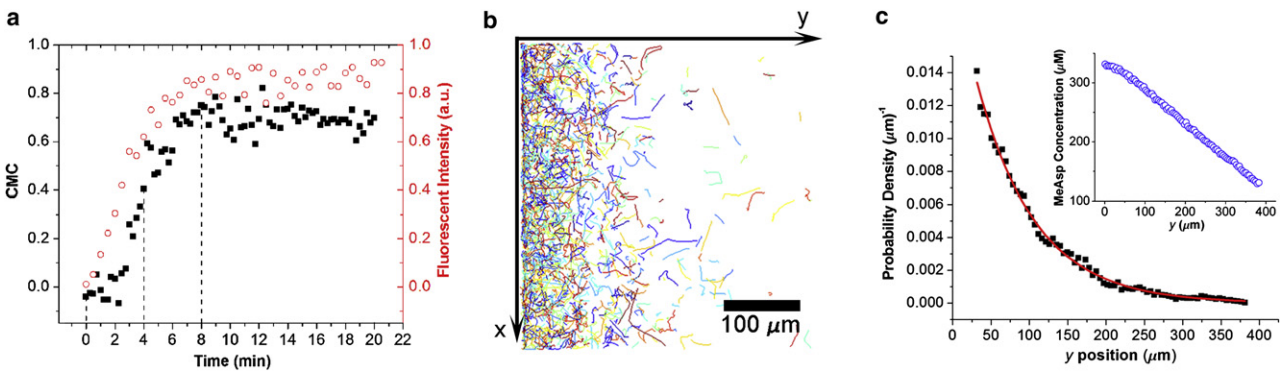

FIGURE 2 A dynamic equilibrium state (*a*). Squares (■) show time evolution of the CMC computed using tracked bacteria positions. The bacterial density distribution reaches a dynamic equilibrium in ~8 min. Circles (●) are the time evolution of chemical concentration gradient in the channel revealed by the fluorescent dye. (*b*). is a graph of 1267 bacterial tracks that was obtained by tracking the steady-state movie shown in Fig. 1 *d*). (*c*). The solid squares represent the measured bacterial cell density profile across the channel at a steady state (t = 20 min). The solid line is an exponential fit to the data. The chemical concentration distribution at this time point is shown in the inset. This curve is obtained using fluorescein solution of 100 μM in the source channel; the *y* axis is scaled to show MeAsp concentration.

Simulation of the cell motion based on its internal pathway dynamics

Since we are interested in describing the population level behavior here, we used a simple coarse-grained model for the internal pathway dynamics. We describe briefly the *E. coli* chemotaxis pathway in the following. The attractant (or repellent) ligand molecules (chemical signal) can bind with the membrane bound Methyl-accepting Chemotaxis Proteins (MCP) chemo-receptors, which form signaling complexes with the histidine kinase protein CheA and the linker molecule CheW. Upon binding to the attractant (repellent) molecules, the chemo-receptors undergo a conformational change that suppresses (increases) the autophosphorylation rate of CheA. In turn, the phosphate group of CheA-P is transferred to the reponse regulator CheY. Once phosphorylated, CheY-P can bind with the motor switch to change the direction of the flagellar motor rotation from counter-clockwise (CCW) to clockwise (CW), which causes the cell to switch from swimming smoothly (run) to wiggling motion (tumble). Thus higher concentrations of attractant molecules can lengthen the run time of the cell. As a result, the cells perform random walks with a bias toward regions with higher concentrations of attractant. The adaptation of the sensory system to persistent stimuli is important for the cells to perform chemotaxis in a wide range of backgrounds. For bacterial chemotaxis, adaptation is carried out by receptor methylation/demethylation facilitated by two enzymes CheR/CheB respectively.

The dynamical state of the internal chemotaxis pathway is described in our model by the average kinase activity a(t) and the average methylation level $m(t)\in[0,4]$ of the MCP receptors, the external environment is given by the ligand concentration $[L](\vec{r})$ at spatial position $\vec{r}$. Receptor ligand binding affects the kinase activity almost immediately while adaptation occurs through receptor methylation at a longer time scale. The kinase activity controls the tumble-and-run motion of the cell by regulating the flagellar motor's probability $p(a)$ for CCW or CW rotation. The cell tumbles when the motor is in the CW state and it moves smoothly (subject to rotational diffusion due to Brownian fluctuation) when the motor is in the CCW state. The resulting motion advances the cell to a new position in space. For a spatial-dependent ligand profile, such as the steady-state linear ligand gradient studied here, the new position of the cell leads to a new ligand concentration that the cell senses and the simulation of both the internal pathway dynamics and the cell motion continues. A flow chart of the simulation is shown in Fig. 3, where the major steps and key variables of our model are illustrated. Quantitative details of our model are explained in the following text.

The kinase activity in our simulation is described by the Monod-Wyman-Changeux two-state model, which captures the essence of receptor cooperativity and has been shown recently (27,28) to generate quantitative agreement with in vivo kinase activity measurements. Each functional MCP receptor complex can be either in the active or the inactive states, these two states are separated by a free energy difference $N\in(m,[L])$, where N is the number of responding receptor dimers in the MCP signaling complex. The average activity is therefore: $a=(1+\exp(N\in(\mathrm{m},[L])))^{-1}$. By using the Monod-Wyman-Changeux model, the free energy difference can be written as: $\in(m,[L])=f_m(m)+1\mathrm{n}(1+[\mathrm{L}]/K)-1\mathrm{n}(1+C[L]/K)$, where $f_m(m)$is the methylation level dependent free energy difference, and K and K/C are the dissociation constants of the ligand to the inactive and the active receptor respectively. For MeAsp, these model parameters were determined in (34) by fitting to the FRET data (20): $N_{\mathrm{Tar}}=6, K=18\mu M, C=0.006$. The free energy contribution due to methylation of the receptor is taken to be linear in m: $f_m(m)=\alpha(m_0-m)$ suggested by recent experimental work ((35); Tom Shimizu, Harvard University, personal communication, 2008). The parameters α and m_0 can be estimated from the dose response data (20,36) of the CheRB- mutants at different methylation levels. For MeAsp, they are roughly $\alpha\approx1.7, m_0\approx1$. The kinetics of the methylation level is taken to have the simple linear form: $dm/dt=k_R(1-a)-k_Ba$, where $k_R(k_B)$ are the rates of methylation (de-methylation) for the inactive (active) receptors as suggested by near perfect adaptation of the system (4, 29-31). More complicated nonlinear Michaelis-Menten equations (37) can also be used, but should not affect the results here. For a gradual ligand gradient, cells always have their activity near their preferred level where the linear form in a is a good approximation. We take $k_R = k_B$ to fix the steady-state activity $a_0 = 0.5$.The methylation rates can then be estimated by the adaptation time in experiments using the step function stimuli (38) for MeAsp, which gives us $k_R \approx 0.005$/s. A general model of the internal pathway dynamics was constructed recently to study the *E. coli* chemotaxis response to temporally varying signals (39). Here we use this pathway model together with a simple model for cell motility (motor response) to study cell *E. coli* chemotaxis behavior in spatially varying chemical profiles.

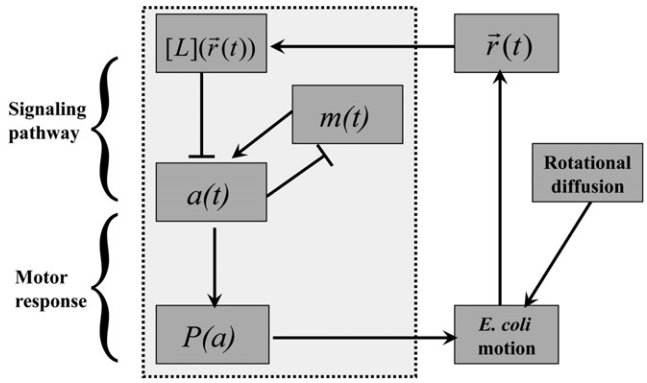

FIGURE 3 Flow chart for the multi-scale theoretical model. The diagram shows steps in our simulation of *E. coli* chemotaxis based on the signaling pathway dynamics and the flagellar motor response (shown in the box with the dotted line). See text for detailed description.

The movement of an *E. coli* cell in our simulation follows the stochastic run-and-tumble pattern. At any given time, a cell can be either moving smoothly (subject to rotational diffusion caused by Brownian fluctuation of the medium) with a run speed $v_0\approx15\mu m$/s as measured in experiments or tumbling. The duration time of the tumble is short and set to be a constant $\tau_1\approx0.2$ s in our model, the cell chooses a random direction to run after each tumble. When the cell is running, the (instantaneous) probability rate of going into the tumbling state is $P(a)$, which depends on the kinase activity, $a(t)$, determined by the pathway model described above. We set the tumbling probability the same as the experimentally measured flagellar CW bias (40), which is $p(a)=\tau_1^{-1}(a/a_{1/2})^H$,where $H\approx10$ is the Hill coefficient of the motor response function. We assume CheY-P level is proportional to the kinase activity. At steady state we have $a=a_0=0.5$ and the cell spends roughly 80% of time running, from which we can determine $a_{1/2}\approx a_o\times4^{1/H}=0.69$. The rotational diffusion constant is set to be 0.28 rad^2/s so that the average directional change in 1 s is roughly 30° in accordance with experiments (4,18).

The boundary condition for moving cells is not well understood, which could be a main source of discrepancy between model and experiments. We assume a quasi-reflective boundary based on the experimental observation. That is, when a cell hits a boundary, it sticks to the boundary for 1 s, and then leaves the boundary with an arbitrary angle.

The coarse-grained model used here contains all the relevant components of the underlying signaling pathway with a small number of parameters, which can all be determined by using data from other independent in vivo experiments. Since we focused on understanding the (averaged) population level behavior of the cells, such coarse-grained model should be sufficient. We have tested the effects of intrinsic noise on the averaged behavior of the cells by including cell to cell variation of the key parameters, such as the methylation/demethylation rates (k_R and k_B) according to experimentally observed distributions (41). We have found no significant changes in the population averaged behavior, such as the steady-state cell density distribution in a given ligand concentration profile. Because of its simplicity, our model has the advantage of being fast computationally as compared with the methods of simulating the internal pathway at individual molecule level

(42, 43), making it possible to study the dynamics of large number of individual cells.

RESULTS

Swimming *E. coli* cells established a dynamic equilibrium in a linear chemical gradient

Upon the addition of the chemoattractant (either MeAsp or L-Serine) along the sink and source channels at t = 0, two processes took place simultaneously. 1), A chemical gradient was established in the center channel via diffusion and it reached a steady state in ~8 min; 2), the pre-seeded bacteria started to migrate toward the region where the chemoattractant concentration was higher. This process continued until a dynamic equilibrium was reached when the chemotactic cell migration was balanced by the cell density diffusion process. This dynamic equilibrium allowed us to take a large amount of data, and quantified the chemotactic response to a high degree of accuracy. To describe this dynamic equilibrium mathematically in the spirit of the Keller-Segel model (44), we assume that the flux (number of cells passing through an unit area in x–z plane) along $-y$ direction due to chemotactic migration is nv_d, and the flux along +y direction due to diffusion as a result of spatial cell density variation is $-\mu(grad(n))$. To the first order of approximation, the dynamic equilibrium state gives us: $nv_d = -\mu(grad(n))$, where n is the cell density, v_d is the average cell drift velocity due to the chemotactic migration, μ is the motility constant of swimming *E. coli* and the axes are defined in Fig. 1 *b*. The solution of this equation is $n=n_0\exp(-(vd/\mu)y)$ where n_0 is the cell density at the edge of the channel y = 0. This exponential relation was demonstrated in our experimental data (Fig. 2 *c* and Fig. 5 (*E1-2*)) as well as model simulation (Fig. 5(*T1-2*)). The measured exponential decay constant, v_d/μ, as well as the chemotactic migration coefficient CMC were used as the measure of the chemotactic responses in both experiments and model simulation. The average chemotactic drift velocity v_d is a more precise measure of the chemotactic response; however, measurements of $v_d$in our experimental setting were impaired by the influence of boundary conditions in the low response region. We therefore used CMC as a measure of the chemotactic response in the broad concentration region and the average drift velocity v_d in the high chemotactic response region (CMC$\geq$ (1/2) CMC_{max}).

Cell concentration dependence of bacterial chemotaxis

To choose an optimal overall cell density $\overline{n}$ for the experiments, we measured the CMC at various cell densities. Fig. 4 shows that the CMCs are kept a constant in the region when the cell density is between 10^7–$5\text{x}10^8$ /mL. We selected 1.5×10^8 /mL for all our experiments as it provides enough statistical data while at the same time the effects of cell-cell interactions and limitations of our tracking program can be ignored.

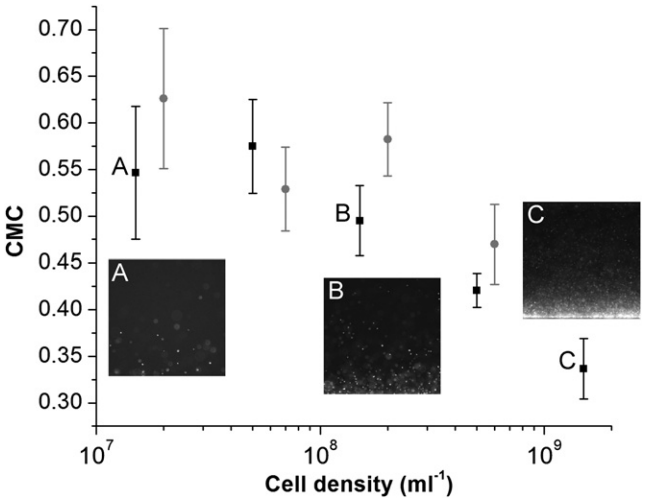

FIGURE 4 Cell density dependence in bacterial chemotaxis CMC measured at various overall cell densities. The black (*gray*) data points were taken when the L-Serine concentration in the source channel is 100 μM (30 μM). A buffer is flowing in the sink channel for all the data points shown. (*A–C*) are actual images of cells in steady state at cell density 1.5×10^7/mL, 1.5×10^8/mL and 1.5×10^9/mL, respectively.

Bacteria's responses in various ligand concentration profiles

To check the hypothesis that bacteria sense the relative change of the ligand concentration, $grad[L]/\overline{[L]}$, we varied $grad[L]$ independently of $\overline{[L]}$ in both experiments and theory. We first kept $\overline{[L]}$ a constant, and varied $grad[L]$(Fig. 5 (*E1,T1*)); and then we kept $grad[L]$ a constant, and changed $\overline{[L]}$ (Fig.5 (*E2, T2*)). Fig. 5(*E1, T1*) shows that the cell density curves become steeper as the spatial gradient of the MeAsp concentration increases, indicating the chemotactic sensitivity increases with $grad[L]$. Fig. 5 (*E2, T2*) shows that the cell density curves become less steep as the average MeAsp concentration increases, indicating the cell chemotactic sensitivity decreases with $\overline{[L]}$. The agreement between cell density profiles from experiments and the model simulation is excellent for most part of the channel, with an exception that the cell density profiles near the channel boundary is flatter in theory than those observed in experiments, probably due to the oversimplification in the boundary condition we used in the model.

Logarithmic sensing of the bacterial chemosensory system

To explore the relation of chemotactic response with $grad[L]/\overline{[L]}$ quantitatively, we fit the cell density curves in Fig. 5 with an exponential decay function (see sample fit in Fig. 2 *c*). Fig. 6 shows that the decay constant increases monotonically with $grad[L]/\overline{[L]}$, and the results from model

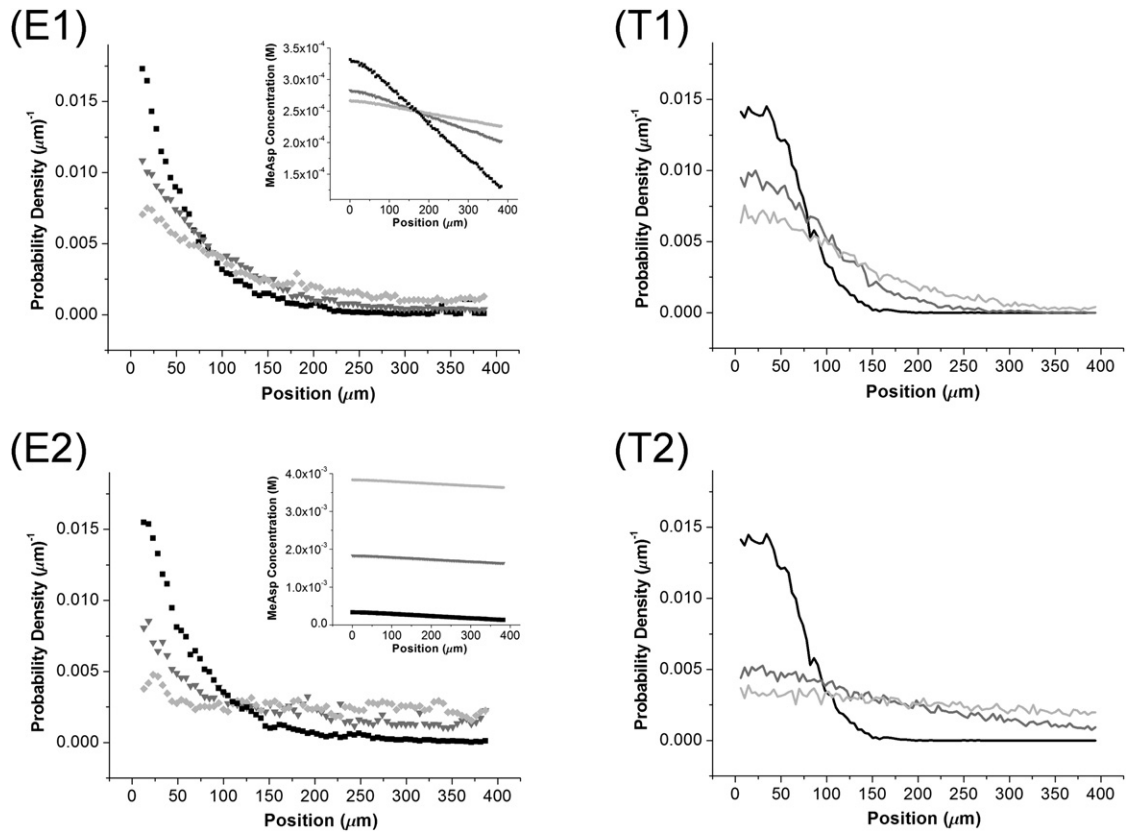

FIGURE 5 *E. coli* density distribution in the vicinity of the peak chemotactic response. (*E1–2*) are distributions obtained in experiments and (*T1–2*) are data from model simulation. (*E1*) and (*T1*): The average chemical concentration is kept a constant, and the chemical gradient is varied; (*E2*) and (*T2*): The chemical gradient is kept a constant, and the average chemical concentration is varied. The insets are the chemo-attractant concentration profiles across the channel, which uses the same color code scheme as the density profiles.

simulation (*triangle symbols with solid line through them*) agree quantitatively with the experimental results (*square symbols*). As mentioned earlier, the decay constant is the average cell chemotactic migration speed v_d divided by the cell motility constant μ. We measured the motility constant μ using the bacterial tracks obtained in experiments (15). We have found that μ is essentially a constant in the set of MeAsp concentrations shown in Fig. 6, which is between 125–150 μm^2/s. Fig. 6 thus shows that the average drift velocity v_d, approximately, increases with $grad[L]/\overline{[L]}$.

Note that $grad[L]/\overline{[L]}$ is used to characterize the average drift velocity, v_d, instead of the local $grad[L]/[L]$, which varies slightly across the channel by ~2-fold in the extreme case. To explore the influences of this variation on the experimental results, we calculated $grad[L]/\overline{[L]}_w$ using a cell distribution weighted average $\overline{[L]}_w = \int \rho(y)[L]dy$, instead of the average value of the chemical concentration in sink and source channels $\overline{[L]} = (1/2)([L]_{\text{source}} + [L]_{\text{sink}})$. The results are shown in the gray dots and lines in Fig. 6. It can be seen that the experimental data agrees better with the theory when using cell density weighted average concentration. For the sake of separating measured values with the controlled parameters, we will use the average concentration as our controlling parameter in the rest of the article.

Bacterial chemotactic response curves

In Fig. 6, we established that the decay constant is monotonically related to $grad[L]/\overline{[L]}$. We now ask how the chemotactic response depends on the average MeAsp concentration when $grad[L]/\overline{[L]}$ is a constant. In this series of experiments and model simulations, we kept $grad[L]/\overline{[L]}$ a constant, and varied $\overline{[L]}$. Experiments were carried out for both MeAsp and L-Serine, while comparison with model prediction was done for MeAsp as the microscopic parameters are better known for MeAsp than for L-Serine. We kept the chemical concentration in the sink channel at 0 (chemotaxis buffer), varied the chemical concentration in the source channel, and thus $grad[L]/\overline{[L]}$ was fixed at (1/450) μm^{-1} (note the distance between the sink and the source channel is 900 μm). Fig. 7 shows that the high chemotactic response region (CMC$\geq$ (1/2) CMC$_{\text{max}}$) covers ~3 orders of magnitude of $\overline{[L]}$ for both MeAsp (10 μM–10 mM) and L-Serine (1 μM–1 mM). In our model simulation (see *solid line* in Fig. 7), the corresponding CMC for MeAsp is about an order of magnitude wider than in the experiments. This can be due

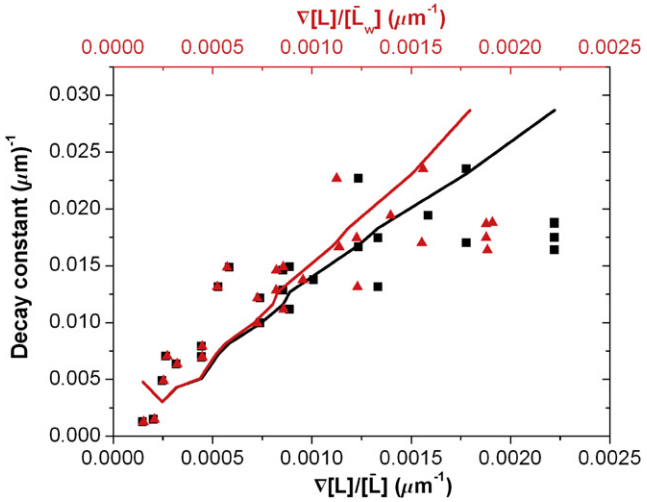

FIGURE 6 Logarithmic sensing of the *E. coli* bacterial chemotaxis. The decay constant or v_d/μ, from the exponential fits versus $grad[L]/\overline{[L]}$ near the peak chemotactic response region. The scattered data points are from experiments, and the solid lines are from the numerical simulation. The gray triangles along with the gray line represent the results where the average concentration $\bar{L}_w$ is weighted by cell density distribution. In all cases, MeAsp is used as a chemoattractant.

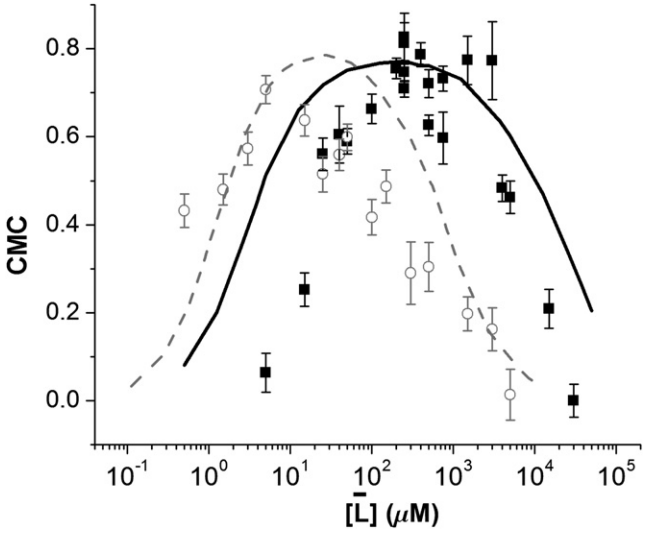

FIGURE 7 Chemotactic response curves. The chemotactic response CMC as a function of average chemoattractant concentration in the center channel when $grad[L]/\overline{[L]}$ is kept constant. Solid squares (■) are experimental data points using MeAsp as chemo-attractant, open circles (○) are experimental data points using L-Serine as chemo-attractant, and the solid line is the model simulation for MeAsp using microscopic parameters from independent experiments. The dashed line is a fit to the experimental data for L-Serine response using adjustable microscopic parameters, and the fitted parameters are $N_{Tsr} = 12$, $K = 6$ μM, $K/C = 30$ μM. For all the data points shown, the chemical concentration in the sink channel is kept at 0, and the chemical concentration in the source channel is varied. Each data point is an average of chemo-index from 500 images, and the error bars are the standard deviations among the 500 CMCs.

to the low detection accuracy at lower chemotactic sensitivity region for experiments and/or the boundary conditions used in the theory. In the case of L-Serine response, there are not enough in vivo kinase response measurements, such as FRET experiments, to determine the microscopic parameters for the Tsr receptor, which is responsible for chemotaxis response to L-Serine. We thus obtained the microscopic parameters for Tsr by matching the simulation results with data from our microfluidics experiments (see the *dashed line* in Fig. 7). This provides us with the predicted microscopic parameters for Tsr receptor and its functional cluster size. The best fitted parameters are found to be N_{Tsr}=12, K=6μM,K/C=30μM The fitted parameter of N_{Tsr}=12 taken together with the previously determined value of N_{Tar}=6 matches the in vivo Tsr:Tar stoichiometry of 2:1, and the total of 18 dimers matches the number of dimers in the hexagonal ring of trimers of dimers observed in the tomography study by Khursigara et al. (45).

The role of adaptation in logarithmic sensing

In exploring the molecular origin of logarithmic sensing, we calculated the steady-state receptor methylation level $\overline{m}$ (averaged over all the cells in the channel) from our model for different average ligand concentration $\overline{[L]}$ using all the ligand profiles studied here (see the section on model simulation for details of the methylation dynamics studied in this study). Fig. 8 demonstrates a linear relation between the average methylation level and the logarithm of the ligand concentration in a wide range of ligand concentration. This suggests that methylation level of the receptors, serving as the ''memory'' of the *E. coli* cells, records the ligand concentration in logarithmic scale. In experiments, we measured the chemotactic response curve (similar to the one shown in Fig. 7) using a mutant that lacks the ability to adapt (RP2867 from Sandy Parkinson, CheRB-). Our preliminary data indicated that the response curve has a very narrow peak (5μM–50μM) which was limited by the resolution of the average concentration in our experiments. Current work is in progress to explore the role of adaptation using the CheRB- mutant in greater details.

DISCUSSION

Two important questions in the *E. coli* chemosensory system have been addressed by combining quantitative results from a microfluidic cell migration assay and a multi-scale theoretical model. First, we showed that the *E. coli* bacteria sense the relative changes of the ligand concentration, instead of its absolute gradient in both experiments and model simulation. This is a common property of biological sensory systems, especially for those that need to process a wide range of signal strengths (such as sensory systems for higher organisms); the logarithm of the signal strength simply compacts a wide range of signal into a manageable one. Weber's law for bacterial chemotaxis, a quantitative description of the sensory system, was first proposed by several

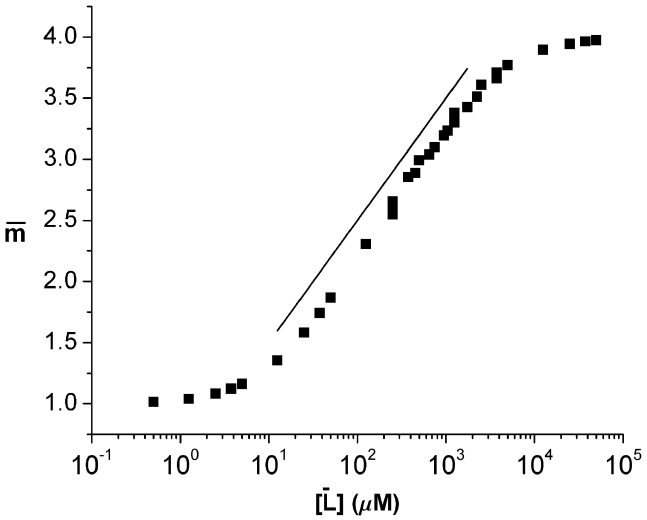

FIGURE 8 Role of adaptation in logarithmic sensing. The mean methylation level $\overline{m}$ (averaged over all the cells in a simulation) is plotted against the average ligand concentration $\overline{[L]}$ in a semi-log plot. The linear regime (indicated by the *solid guideline*) in the intermediate range of the ligand concentration corresponds to the logarithmic sensing of the chemotaxis pathway.

groups based on qualitative chemotaxis assays with not precisely controlled time-dependent ligand profiles more than 30 years ago. We show for the first time, to our knowledge, that the characteristic drift velocity, the key characteristics of the *E. coli* chemo-response, depends on $grad[L]/\overline{[L]}$, in a wide range of controlled ligand profiles, i.e., the *E. coli* cells sense the gradient of the logarithmic ligand concentration. Our theoretical model, with all its parameters determined from independent in vivo experiments, predicts the same behavior as observed in the experiments. This quantitative agreement between the cell level measurements and the pathway-based model not only verifies the model; the model, more importantly, makes it possible to understand the macroscopic cellular behaviors by the underlying microscopic pathway kinetics. The previous argument based entirely on receptor occupancy changes is clearly inadequate to explain the broad range of high sensitivity observed here (3, 4). From our study, the logarithmic sensing of the ligand concentration is caused by adaptation and the way methylation of the chemo-receptor affects the kinase activity. As shown in recent in vivo experiments (20,36) that are incorporated into our model, changes in receptor methylation level simply shift the steady curves of the kinase-activity versus ligand in semi-log scale without altering their shape, i.e., a given receptor methylation level increment can balance a corresponding fold increase in ligand concentration to keep the kinase activity constant. Therefore, to maintain the kinase activity near its preferred operation point (near perfect adaptation), the adaptation dynamics drives the receptor methylation level to follow the logarithm of the external ligand concentration. Considering the large range of ligand concentrations the cell is likely to encounter and the limited bandwidth (methylation levels) for recording, this logarithmic transformation of the signal is a sensible strategy for the *E. coli* to survive in a diverse environment. The logarithmic dependence of $\overline{m}$ on $\overline{[L]}$ is a prediction of our model and should be tested experimentally by measuring the average receptor methylation level in different ligand backgrounds.

Second, we have determined by both experiments and theory the exact regions of ligand concentration where high sensitivity (defined as ($CMC \geq (1/2)\ CMC_{max}$)) is observed for MeAsp and L-Serine. These regions are found to be much wider than those predicted by the ligand occupancy based argument. For MeAsp, we find that there is a plateau at maximum sensitivity for two orders of magnitude between 25μM and 3mM in experiment. This range can be explained microscopically by our theory where the region of the plateau is spanned by the two receptor-ligand dissociation constants K and K/C for inactive and active receptors respectively. Quantitatively, these two dissociation constants, found to be 18μM and 3 mM in an earlier work (34) by fitting to in vivo FRET measurements, are in excellent agreement with the current observation. In addition, the overall high sensitivity region measured in experiment spans about three decades of the average ligand concentration. In theory, the receptor cooperativity, characterized by the number of receptor N in the functional cluster, is known to extend the high sensitivity region (the flanking region) around the plateau by a factor proportional to N, which results to the overall high sensitivity region to be around four decades. In this case, $N_{Tar} \approx 6$ has been determined for MeAsp from the same previous study (34). For very small and very large ligand concentrations, the theory and experiments start to differ appreciably. We believe that they could be due to effects of fluctuations for the low ligand concentration cases and the boundary effects/the approximate boundary conditions in the experiments/model. For L-Serine response, our experimental results are used to determine the microscopic parameters that have not been measured before. We found the two dissociation constants K and K/C for L-Serine to be roughly 6μM and 30μM respectively, spanning a much smaller region than that of the MeAsp response. This may explain the earlier experimental finding that *E. coli* fails to adapt exactly to large concentrations of L-Serine (46).

Put together, we have now a quantitative understanding of how *E. coli* cells respond to different spatial ligand profiles and its dynamic range. The combination of the quantitative cell behavior assay and the internal pathway dynamics based model is critical in connecting molecular mechanism to cellular behavior. It establishes a new paradigm in investigating other important phenomena in *E. coli* chemotaxis, such as signal integration and differentiation in more complex/realistic environment. It may also be applicable to other relevant biological problems that are of direct biomedical applications, such as directed cell migration in higher organisms. Increasing evidence has shown mammalian cell

migration depends sensitively on its chemical environment, in particular on the number of ligand-receptor binding sites (16,47). However, the quantitative understanding of the internal signaling pathway dynamics, such as the adaptation system, for many of these mammalian cells is still at its infancy. The lessons we have learned in *E. coli* bacteria chemotaxis on logarithmic sensing may provide insights on the underlying molecular mechanisms with which eukaryotic cells migrate.

The authors thank John S. Parkinson for providing the bacterial strains (RP437), Matthew DeLisa for providing the GFP bacterial strains (RP437), and Howard Berg and Linda Turner for very helpful discussions.

This work was supported, in part, with funds from the National Science Foundation (CBET-0619626) and the New York State Office of Science, Technology and Academic Research (NYSTAR) (in the form of a Center for Advanced Technology grant), and by grants from the Nanobiotechnology Center (NBTC), a Science and Technology Center Program of the National Science Foundation under Agreement No. ECS-9876771 for Y.K. and M.W. The work by Y.T. is partially supported by a National Institutes of Health grant (1R01GM081747-01).

REFERENCES

1. Thompson, R. F. 1967. Foundations of physiological psychology. Harper and Row, New York.
2. Dahlquist, F. W., P. Lovely, and D. E. Koshland. 1972. Quantitative analysis of bacterial migration in chemotaxis. *Nat. New Biol.* 236:120–123.
3. Mesibov, R., G. W. Ordal, and J. Adler. 1973. Range of attractant concentrations for bacterial chemotaxis and threshold and size of response over this range - Weber Law and related phenomena. *J. Gen. Physiol.* 62:203–223.
4. Brown, D. A., and H. C. Berg. 1974. Temporal stimulation of chemotaxis in Escherichia coli. *Proc. Natl. Acad. Sci. USA.* 71:1388–1393.
5. Jasuja, R., L. Yu, D. R. Trentham, and S. Khan. 1999. Response tuning in bacterial chemotaxis. *Proc. Natl. Acad. Sci. USA.* 96:11346–11351.
6. Ahmed, T., and R. Stocker. 2008. Experimental verification of the behavioral foundation of bacterial transport parameters using microfluidics. *Biophys. J. BioFAST. 10.1529/biophysj.108.134510.*
7. Mao, H. B., P. S. Cremer, and M. D. Manson. 2003. A sensitive, versatile microfluidic assay for bacterial chemotaxis. *Proc. Natl. Acad. Sci. USA.* 100:5449–5454.
8. Tindall, M., S. Porter, P. Maini, G. Gaglia, and J. Armitage. 2008. Overview of Mathematical Approaches Used to Model Bacterial Chemotaxis I: The Single Cell. *Bull. Math. Biol.* 70:1525–1569.
9. Tindall, M., P. Maini, S. Porter, and J. Armitage. 2008. Overview of Mathematical Approaches Used to Model Bacterial Chemotaxis II: Bacterial Populations. *Bull. Math. Biol.* 70:1570–1607.
10. Falke, J. J., and G. L. Hazelbauer. 2001. Transmembrane signaling in bacterial chemoreceptors. *Trends Biochem. Sci.* 26:257–265.
11. Sourjik, V., and H. C. Berg. 2000. Localization of components of the chemotaxis machinery of *Escherichia coli* using fluorescent protein fusions. *Mol. Microbiol.* 37:740–751.
12. Weibel, D. B., W. R. DiLuzio, and G. M. Whitesides. 2007. Microfabrication meets microbiology. *Nat. Rev. Microbiol.* 5:209–218.
13. Dertinger, S. K. W., D. T. Chiu, N. L. Jeon, and G. M. Whitesides. 2001. Generation of gradients having complex shapes using microfluidic networks. *Anal. Chem.* 73:1240–1246.
14. Wu, M., J. W. Roberts, and M. Buckley. 2005. Three-dimensional fluorescent particle tracking at micron-scale using a single camera. *Exp. Fluids.* 38:461–465.
15. Wu, M., J. W. Roberts, S. Kim, D. L. Koch, and M. P. DeLisa. 2006. Collective bacterial dynamics revealed using a three-dimensional population-scale defocused particle tracking technique. *Appl. Environ. Microbiol.* 72:4987–4994.
16. Wong K. A. Ayuso-Sacido, P. Ahyow, A. Darling, J. A. Boockvar, et al. 2008. Assessing neural stem cell motility using an agarose gel based microfluidic device. *Journal of Visualized Experiments*: http://www.jove.com/index/Details.stp%3FID%3D674.
17. Cheng, S. -Y., S. Heilman, M. Wasserman, S. Archer, M. L. Shuler, et al. 2007. A hydrogel-based microfluidic device for the studies of directed cell migration. *Lab Chip.* 7:763–769.
18. Berg, H. C. 2000. Motile behavior of bacteria. *Phys. Today.* 53:24–29.
19. Bren, A., and M. Eisenbach. 2000. How signals are heard during bacterial chemotaxis: Protein-protein interactions in sensory signal propagation. *J. Bacteriol.* 182:6865–6873.
20. Sourjik, V., and H. C. Berg. 2002. Receptor sensitivity in bacterial chemotaxis. *Proc. Natl. Acad. Sci. USA.* 99:123–127.
21. Vaknin, A., and H. C. Berg. 2004. Single-cell FRET imaging of phosphatase activity in the *Escherichia coli* chemotaxis system. *Proc. Natl. Acad. Sci. USA.* 101:17072–17077.
22. Sourjik, V., and H. C. Berg. 2004. Functional interactions between receptors in bacterial chemotaxis. *Nature.* 428:437–441.
23. Maddock, J. R., and L. Shapiro. 1993. Polar location of the chemoreceptor complex in the *Escherichia coli* cell. *Science.* 259:1717–1723.
24. Bray, D., M. D. Levin, and C. J. Morton-Firth. 1998. Receptor clustering as a cellular mechanism to control sensitivity. *Nature.* 393:85–88.
25. Duke, T. A. J., and D. Bray. 1999. Heightened sensitivity of a lattice of membrane receptors. *Proc. Natl. Acad. Sci. USA.* 96:10104–10108.
26. Mello, B. A., and Y. H. Tu. 2003. Quantitative modeling of sensitivity in bacterial chemotaxis: The role of coupling among different chemoreceptor species. *Proc. Natl. Acad. Sci. USA.* 100:8223–8228.
27. Mello, B. A., and Y. H. Tu. 2005. An allosteric model for heterogeneous receptor complexes: Understanding bacterial chemotaxis responses to multiple stimuli. *Proc. Natl. Acad. Sci. USA.* 102:17354–17359.
28. Keymer, J. E., R. G. Endres, M. Skoge, Y. Meir, and N. S. Wingreen. 2006. Chemosensing in *Escherichia coli*: Two regimes of two-state receptors. *Proc. Natl. Acad. Sci. USA.* 103:1786–1791.
29. Mello, B. A., and Y. Tu. 2003. Perfect and near-perfect adaptation in a model of bacterial chemotaxis. *Biophys. J.* 84:2943–2956.
30. Barkai, N., and S. Leibler. 1997. Robustness in simple biochemical networks. *Nature.* 387:913–917.
31. Yi, T. M., Y. Huang, M. I. Simon, and J. Doyle. 2000. Robust perfect adaptation in bacterial chemotaxis through integral feedback control. *Proc. Natl. Acad. Sci. USA.* 97:4649–4653.
32. Diao, J. P., L. Young, S. Kim, E. A. Fogarty, S. M. Heilman, et al. 2006. A three-channel microfluidic device for generating static linear gradients and its application to the quantitative analysis of bacterial chemotaxis. *Lab Chip.* 6:381–388.
33. Liao, Q., G. Subramanian, M. P. DeLisa, D. L. Koch, and M. Wu. 2007. Pair velocity correlations among swimming *Escherichia coli* bacteria are determined by force-quadrupole hydrodynamic interactions. *Phys. Fluids.* 19:061701–061705.
34. Mello, B. A., and Y. H. Tu. 2007. Effects of adaptation in maintaining high sensitivity over a wide range of backgrounds for *Escherichia coli* chemotaxis. *Biophys. J.* 92:2329–2337.
35. Vaknin, A., and H. C. Berg. 2007. Physical responses of bacterial chemoreceptors. *J. Mol. Biol.* 366:1416–1423.
36. Shimizu, T. S., N. Delalez, K. Pichler, and H. C. Berg. 2006. Monitoring bacterial chemotaxis by using bioluminescence resonance energy transfer: Absence of feedback from the flagellar motors. *Proc. Natl. Acad. Sci. USA.* 103:2093–2097.
37. Emonet, T., and P. Cluzel. 2008. Relationship between cellular response and behavioral variability in bacterial chemotaxis. *Proc. Natl. Acad. Sci. USA.* 105:3304–3309.

38. Berg, H. C., and P. M. Tedesco. 1975. Transient response to chemotactic stimuli in. *Escherichia coli*. *Proc. Natl. Acad. Sci. USA*. 72:3235–3239.

39. Tu, Y., T. S. Shimizu, and H. C. Berg. 2008. Modeling the chemotactic response of *Escherichia coli* to time-varying stimuli. *Proc. Natl. Acad. Sci. USA*. 105:14855–14860.

40. Cluzel, P., M. Surette, and S. Leibler. 2000. An ultrasensitive bacterial motor revealed by monitoring signaling proteins in single cells. *Science*. 287:1652–1655.

41. Kollmann, M., L. Lovdok, K. Bartholome, J. Timmer, and V. Sourjik. 2005. Design principles of a bacterial signalling network. *Nature*. 438:504–507.

42. Emonet, T., C. M. Macal, M. J. North, C. E. Wickersham, and P. Cluzel. 2005. AgentCell: a digital single-cell assay for bacterial chemotaxis. *Bioinformatics*. 21:2714–2721.

43. Le Novere, N., and T. S. Shimizu. 2001. STOCHSIM: modelling of stochastic biomolecular processes. *Bioinformatics*. 17:575–576.

44. Keller, E. F., and L. A. Segel. 1971. Model for chemotaxis. *J. Theor. Biol*. 30:225–234.

45. Khursigara, C. M., X. Wu, P. Zhang, and S. Subramaniam. 2008. Role of HAMP domains in chemotaxis signaling by bacterial chemoreceptors. *Proc. Natl. Acad. Sci. USA.,* In press.

46. Berg, H. C., and D. A. Brown. 1972. Chemotaxis in *Escherichia Coli* Analyzed by 3-Dimensional Tracking. *Nature*. 239:500–504.

47. Pedersen, M. W., V. Tkach, N. Pedersen, V. Berezin, and H. S. Poulsen. 2004. Expression of a naturally occurring constitutively active variant of the epidermal growth factor receptor in mouse fibroblasts increases motility. *Int. J. Cancer*. 108:643–653.